TSINGHUA SCIENCE AND TECHNOLOGY
ISSN 1007-0214 19/23 pp2251–2263
DOI: 10.26599/TST.2024.9010178
Volume 31, Number 4, August 2026

Research Article

Polarization-Aided BP Decoding for Uplink Non-Orthogonal Multiple Access

Yuehui Xu, Xinyang Piao, Zhaopeng Xie*, Yuanping Wang, and Pingping Chen

Abstract: In this paper, we propose a polarization-aided belief propagation (PA-BP) decoding for *M*-user uplink non-orthogonal multiple access (NOMA). In this scheme, polar code of each user is regarded as a nested code within a longer polar code with BP decoding, which has the length *M* times than that of the original user codes. It enables the PA-BP decoder to obtain all user messages with the enhanced channel polarization effect, as compared to the conventional successive interference cancellation BP (SIC-BP) decoder at finite block length. To improve the performance of PA-BP decoder, we further propose interference cancellation (IC) aided-BP (ICA-BP) and ICA-BPL list decoders that incorporates IC during PA-BP iterations. We then analyze the channel capacity of the proposed scheme and use extrinsic information transfer (EXIT) chart to show the convergence behavior of these iterative decoders. By utilizing the Monte Carlo method to optimize this long polar code, simulation results show that the proposed PA-BP outperforms the conventional SIC-BP by 0.8 dB over Gaussian channels, and by 0.7 dB over Rayleigh fading channels. In particular, ICA-BP can achieve more performance gain of 0.4 dB over PA-BP over both channels.

Key words: polarization effect; belief propagation (BP); non-orthogonal multiple access (NOMA); successive interference cancellation (SIC)

1 Introduction

Non-orthogonal multiple access (NOMA) has gained significant attention due to its ability to improve spectrum efficiency and system throughput[1–3]. Unlike orthogonal multiple access (OMA), which allocates orthogonal resources to individual users, NOMA allows for the superimposition of multiple users and subsequent separation using successive interference cancellation (SIC) decoders at the receiver[4–6]. This method decodes information in order of user strength while mitigating interference from previously decoded results. The existing NOMA schemes can be classified into two categories: power domain NOMA and code domain NOMA[7–9]. In power domain NOMA, users are differentiated based on their individual channel conditions[10]. Users with favorable channel conditions are referred to as strong users, while those with less favorable conditions are classified as weak users.

Polar code is the first channel coding scheme that has been mathematically proven to achieve Shannon's channel capacity as the code length approaches infinity[11]. Based on the theorem of channel polarization, the transmitted messages are polarized into reliable information bits and unreliable frozen bits[12]. The successive cancellation (SC) algorithm,

• Yuehui Xu, Yuanping Wang, and Pingping Chen are with College of Physics and Information Engineering, Fuzhou University, Fuzhou 350108, China. E-mail: kobejax123@gmail.com; wyp_yuanping@163.com; ppchen.xm@gmail.com.
• Xinyang Piao is with Department of Electrical Engineering, Columbia University, Manhattan, NY 10027, USA. E-mail: xp2123@columbia.edu.
• Zhaopeng Xie is with School of Advanced Manufacturing, Fuzhou University, Jinjiang 362251, China. E-mail: xzp_fzu@163.com.
* To whom correspondence should be addressed.
Manuscript received: 2024-06-26; revised: 2024-08-03; accepted: 2024-09-19

proposed by Arikan, is commonly used for sequential decoding. The ultra reliable and low-latency communications (uRLLC), which is one of the services to be supported by 5G, has raised the demands for low latency decoding in NOMA system[13–15]. However, the SC decoders introduce inevitable latency and fail to fully utilize hardware resources due to their serial nature[16]. To address this issue, a belief propagation (BP) decoder is proposed in Ref. [17], which not only reduces latency but is also more hardware-friendly.

Numerous studies have explored the collaboration between polar codes and NOMA. In Ref. [18], a framework was presented to optimize binary polar coding and multi-carrier NOMA. Ref. [4] introduced polar-coded NOMA (PC-NOMA) with special frozen bit patterns. In the uplink communications, each user is assigned a exclusive pattern of frozen bits. It can enhance robustness in the presence of imperfect power control. In Ref. [19], a joint multi-user decoding was proposed for q-ary polar codes to mitigate the effects of channel fluctuations.

Moreover, Ref. [20] introduced a joint polar coding and physical-layer network coding (PNC) scheme for downlink NOMA (PN-NOMA). This scheme incorporates the concept of exclusive OR (XOR) mapping to help polar decoding[21–24].

In this paper, inspired by polar coding structure and the concept of PNC, we propose a polarization-aided belief propagation (PA-BP) decoding in uplink NOMA systems. The user codeword are regarded as nested codes of a longer polar code, which can be derived from the superimposed signals. In contrast to SC, the proposed PA-BP is a hardware-friendly approach for high throughput applications due to its parallel decoding structure. Furthermore, PA-BP is efficient for decoding all user messages within a single decoder, which also enhances both the channel polarization effect and decoding performance.

Our main contributions are concluded as follows:

1) We propose a PA-BP decoding for a two-user uplink NOMA system, where a long codeword is virtually constructed at the receiver from the superimposed signal. The nested short user codes are optimized by using Monte Carlo method. The channel polarization effect and then decoding performance is improved.

2) We analyze the channel capacity of PA-BP and SIC-BP schemes. Moreover, extrinsic information transfer (EXIT) chart is used to illustrate the convergence behavior of the proposed decoders.

3) To enhance the performance of PA-BP, we propose an interference cancellation (IC) aided-BP (ICA-BP) algorithm. Simulation results show the proposed decoding achieves significant performance gain over the conventional SIC-BP decoding schemes.

The remainder of this paper is organized as follows. Section 2 provides a brief review of the system model and polar codes. In Section 3, the framework of PA-BP decoding scheme and Monte Carlo construction are explicitly described. Capacity analysis and EXIT chart are also introduced. In Section 4, ICA-BP decoder is illustrated. Section 5 presents the simulation results and Section 6 concludes the paper.

2 Background and System Model

2.1 System model

Figure 1 illustrates an uplink NOMA communication system in which the base station (BS) receives transmitted signals from M users simultaneously. Let the message for user i be denoted as u_i, and its corresponding codeword after polar encoding with a code length of Z be x_i $(i = 1, 2, \ldots, M)$. Next, x_i is modulated using binary phase shift keying (BPSK) to generate the transmitted signals r_i. Assuming that BS receives the superimposed from all r_i signals simultaneously over a symbol duration, which can be represented as

$$y = \sum_{i=1}^{M} h_i \sqrt{P_i} r_i + \eta \tag{1}$$

where h_i denotes the response for channel conditions between user-i and BS. For Rayleigh fading channels, $h_i = d_i^{-\gamma} g_i$, d_i is the propagation distance from users to BS and γ is the path loss exponent, and

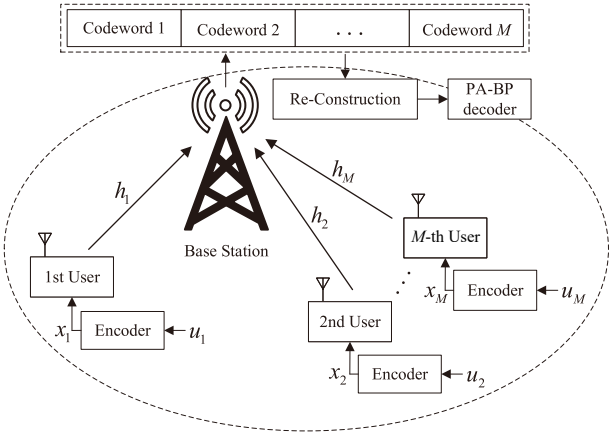

Fig. 1 Model of an uplink NOMA system.

$g_i \sim \mathcal{CN}(0, 1)$[25]. The power level configured by the transmitters is denoted as P_i, and η is the Gaussian white noise, which follows a normal distribution with zero mean and a standard deviation of σ. As seen in Fig. 1, in the proposed PA-BP, there is a single polar decoder constructed at the BS. The codewords of M users can be extracted from the received signal y and then form this single code, which has the length M times than that of the original user codes.

In this paper, we consider an equal power allocation for all users, i.e., $P_i = 1$, $\forall i$. We also assume that the channel state information (CSI) are known at the receiver, which can be obtained from channel estimation, such as channel state feedback strategy or deep learning approach[26, 27].

2.2 Channel polarization

Polar codes are characterized by channel polarization, which depends on their encoding principle. Consider a binary-input discrete memoryless channel (BI-DMC) denoted as $\mathcal{X} \to \mathcal{Y}$, where the input alphabet $\mathcal{X}$ is $\{0, 1\}$. The channel transition probability is denoted as $W(y|x)$, where the transmitted symbol x belongs to the input alphabet $\mathcal{X}$ and the received symbol y belongs to the output alphabet $\mathcal{Y}$. Let a_1^N represent an N-dimensional vector $\{a_1, a_2, \ldots, a_N\}$. The original information block u_1^N comprises the information set $\mathcal{A}$ and the set of frozen bits $\mathcal{A}^c$. Subsequently, the codeword x_1^N is generated by

$$x_1^N = u_1^N G_N \tag{2}$$

where $G_N = F^{\otimes n}$ is obtained from the n-th Kronecker product of the polarization kernel $F = \begin{bmatrix} 1 & 0 \\ 1 & 1 \end{bmatrix}$. The N independent channels are first merged, given by

$$W_N\left(y_1^N|x_1^N\right) = W^N\left(y_1^N|u_1^N \times G_N\right) \tag{3}$$

Subsequently, they are split into bit-channels $W_N^{(i)}$, for $i \in \{1, 2, \ldots, N\}$. Let $W_N^{(i)}\left(y_1^N, u_1^{i-1}|u_i\right)$ denote the i-th channel transition probability with input bit u_i and outputs y_1^N, u_1^{i-1}, given by

$$W_N^{(i)}\left(y_1^N, u_1^{i-1}|u_i\right) \stackrel{def}{=} \sum_{u_{i+1}^N \in \mathcal{X}^{N-i}} \frac{1}{2^{N-1}} W_N\left(y_1^N|u_1^N\right) \tag{4}$$

The reliability of these bit-channels can be estimated and sorted by construction algorithms, such as Monte Carlo method[11] or Gaussian approximation (GA)[28]. Then the K most reliable bit-channels are selected to transmit information bits, while the remaining ones carry frozen bits (typically fixed at 0). The logarithmic likelihood ratio (LLR) for the i-th bit u_i is defined as

$$L_N^{(i)} = \ln \frac{W_N^{(i)}\left(y_1^N, \hat{u}_1^{i-1}|u_i = 0\right)}{W_N^{(i)}\left(y_1^N, \hat{u}_1^{i-1}|u_i = 1\right)} \tag{5}$$

where $\hat{u}_1^{i-1}$ is the estimation of sequence u_1^{i-1} before current bit u_i. Let $u_{1,o}^j$ and $u_{1,e}^j$ denote the sub-vectors of estimated sequence with odd and even indices respectively and define the boxplus operation $a \boxplus b = \ln\left(\left(1 + \mathrm{e}^{(a+b)}\right) / \left(\mathrm{e}^a + \mathrm{e}^b\right)\right)$. Upon receiving initial LLRs from channel output, SC decoder calculates LLRs using the following recursive formulas:

$$\begin{aligned} L_N^{(2i-1)}\left(y_1^N, \hat{u}_1^{2i-2}\right) = & L_{N/2}^{(i)}\left(y_1^{N/2}, \hat{u}_{1,o}^{2i-2} \oplus \hat{u}_{1,e}^{2i-2}\right) \boxplus \\ & L_{N/2}^{(i)}\left(y_{N/2+1}^N, \hat{u}_{1,e}^{2i-2}\right) \end{aligned} \tag{6}$$

$$\begin{aligned} L_N^{(2i)}\left(y_1^N, \hat{u}_1^{2i-1}\right) = & \\ & (-1)^{\hat{u}_{2i-1}} L_{N/2}^{(i)}\left(y_1^{N/2}, \hat{u}_{1,o}^{2i-2} \oplus \hat{u}_{1,e}^{2i-2}\right) + \\ & L_{N/2}^{(i)}\left(y_{N/2+1}^N, \hat{u}_{1,e}^{2i-2}\right) \end{aligned} \tag{7}$$

2.3 BP decoding for polar codes

The factor graph-based belief propagation algorithm was introduced as a parallel and iterative decoding scheme. Its objective is to address the high latency caused by sequential decoding. Furthermore, it can optimize error performance for finite block length, since parallel decoding does not exhibit bit error propagation[29–31].

Two types of messages including left message $\boldsymbol{L}_{i,j}$ and right message $\boldsymbol{R}_{i,j}$ are iteratively propagated through the factor graph[17, 32], where i and j represent the stage and row indices respectively ($1 \leqslant i \leqslant n+1$, $1 \leqslant j \leqslant N$). The factor graph consists of $n+1$ ($n = \log_2 N$) stages and each stage has $N/2$ processing elements (PE). Figure 2 shows a factor graph of $N = 8$ as an example, where the numbers in brackets represent the row and column of each node, facilitating us to locate any node on the factor graph. Before starting iterations, the left messages $\boldsymbol{L}_{n+1,j}$ are assigned as LLR values calculated from the channel outputs, while the right messages $\boldsymbol{R}_{1,j}$ are set to ∞ if $j \in \mathcal{A}^c$, otherwise zero. During each iteration, $\boldsymbol{L}_{i,j}$ and $\boldsymbol{R}_{i,j}$ are updated as follow

$$\begin{aligned} & \boldsymbol{L}_{i,j} = f\left(\boldsymbol{L}_{i+1,j}, \boldsymbol{R}_{i,j+2^{n-1-i}} + \boldsymbol{L}_{i+1,j+2^{n-1-i}}\right), \\ & \boldsymbol{L}_{i,j+2^{n-1-i}} = f\left(\boldsymbol{L}_{i+1,j}, R_{i,j}\right) + \boldsymbol{L}_{i+1,j+2^{n-1-i}} \end{aligned} \tag{8}$$

$$\begin{aligned} & \boldsymbol{R}_{i+1,j} = f\left(\boldsymbol{R}_{i,j}, \boldsymbol{R}_{i,j+2^{n-1-i}} + \boldsymbol{L}_{i+1,j+2^{n-1-i}}\right), \\ & \boldsymbol{R}_{i+1,j+2^{n-1-i}} = f\left(\boldsymbol{L}_{i+1,j}, \boldsymbol{R}_{i,j}\right) + \boldsymbol{R}_{i,j+2^{n-1-i}} \end{aligned} \tag{9}$$

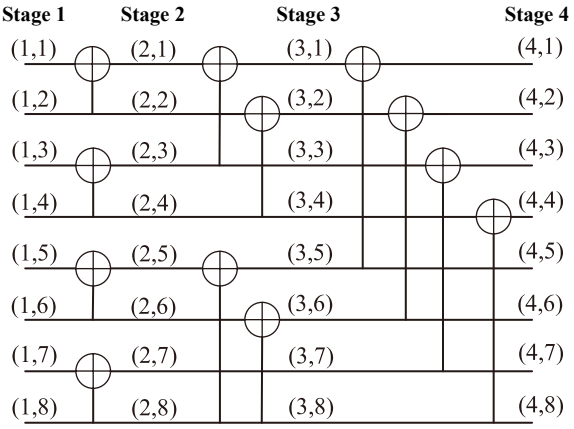

Fig. 2 Factor graph of $N = 8$ polar code.

where $f(a, b)$ is approximated by the scaled min sum (SMS) algorithm

$$f(a, b) \approx \alpha \cdot \text{sign}(a) \cdot \text{sign}(b) \cdot \min\{|a|, |b|\} \tag{10}$$

The coefficient α generally takes the value of 0.9375 for approximation[33]. BP decoder terminates its iterations when a preset maximum number of iterations is reached or the early detection and termination criteria (EDTC) is met, e.g, CRC-based or G-matrix-based criterion[34, 35]. Then decoding output $\hat{u}_1^N$ is evaluated by

$$\hat{u}_j = \begin{cases} 1, & \text{if } \boldsymbol{R}_{1,j} + \boldsymbol{L}_{1,j} < 0, \\ 0, & \text{if } \boldsymbol{R}_{1,j} + \boldsymbol{L}_{1,j} \geqslant 0, \\ 0, & \text{if } j \in \mathcal{A}^c \end{cases} \tag{11}$$

3 Proposed Polarization Aided BP and ICA-BP Decoder

3.1 Polarization aided-BP decoder

According to the linear properties of polar code, an original information block u_1^N can be divided into M code blocks $u_1^N = (u_1^Z, u_{Z+1}^{2Z}, \ldots, u_{(M-1)Z+1}^N)$. Correspondingly, they can be encoded by a generator sub-matrix $\bar{G}_Z = F^{\otimes n-m}$ into sub-codewords $(\bar{x}_1^Z, \bar{x}_{Z+1}^{2Z}, \ldots, \bar{x}_{(M-1)Z+1}^N)$. Then they can be encoded by a joint matrix $\bar{G}_M = F^{\otimes m}$ into x_1^N[20]. Let $Z = N/M$ denote the length of code block, $m = \log_2 M$. The encoding is equivalently given by

$$\begin{aligned} x_1^N =& u_1^N G_N = u_1^N (F^{\otimes n-m} \otimes F^{\otimes m}) = \\ & ((u_1^Z F^{\otimes n-m})^T, (u_{Z+1}^{2Z} F^{\otimes n-m})^T, \ldots, \\ & (u_{(M-1)Z+1}^N F^{\otimes n-m})^T) F^{\otimes n-1} = \\ & ((\bar{x}_1^Z)^T, (\bar{x}_{Z+1}^{2Z})^T, \ldots, (\bar{x}_{(M-1)Z+1}^N)^T) \bar{G}_M \end{aligned} \tag{12}$$

Figure 3 illustrates framework of a two-user uplink NOMA system, where $N = 2Z$. Let $x_{1,i}^Z$ denote the polar codeword for user with index i, $i \in \{1, 2\}$ and $x_{1,o}^Z$ is the XOR of $x_{1,1}^Z$ and $x_{1,2}^Z$. Two users generate their codewords according to the preassigned information set. After polar encoding and BPSK modulation, the messages of the two users are transmitted to the BS through respective channels. In the BS, received codewords of two users can be jointly encoded according to (12), which is given by

$$\begin{aligned} x_{1,B}^N = (\bar{x}_{1,1}^Z, \bar{x}_{1,2}^Z) \begin{bmatrix} 1 & 0 \\ 1 & 1 \end{bmatrix} = \\ (\bar{x}_{1,1}^Z \oplus \bar{x}_{1,2}^Z, \bar{x}_{1,2}^Z) = (\bar{x}_{1,o}^Z, \bar{x}_{1,2}^Z) \end{aligned} \tag{13}$$

where $x_{1,o}^Z$ and $x_{1,2}^Z$ can be considered as nested short codes of a longer polar code $x_{1,B}^N$. Due to the difference of channel gains, LLRs of user 1, 2 and their XOR message can be distinguished and calculated by the XOR mapping rule from the superimposed signals. Notice that BS receives y_1^Z in a symbol duration as

$$y_1^Z = h_1 r_{1,1}^Z + h_2 r_{1,2}^Z + \eta \tag{14}$$

Therefore, four possible types of superimposed signals are assembled into a set $S = \{h_1 + h_2, h_1 - h_2, -h_1 + h_2, -h_1 - h_2\}$, where elements s_j in S have the same a-prior probability $\Pr(s_j) = 1/4$ for $j = 0, 1, 2, 3$.

Upon receiving signal y_1^Z and conditioned on s_j, the transfer probability for k-th bit is

$$p_{k,j} = \Pr(y_k | s_j) = \frac{1}{4\beta\sqrt{2\pi}\sigma} \exp\left(-\frac{|y_k - s_j|^2}{2\sigma^2}\right) \tag{15}$$

where β is a normalization factor to ensure $\sum_{j=0}^{3} p_{k,j} = 1$. Table 1 provides the details of XOR mapping rule between superimposed signals and users' bits. In BS, the k-th bit LLR values for i-th user and XOR message of both users are denoted as $L_{k,i}$ and $L_{k,o}$, respectively, computed by

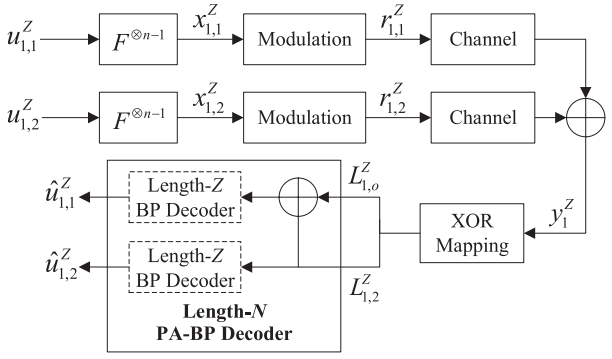

Fig. 3 Block diagram of the PA-BP decoding scheme.

Table 1 PNC mapping rule for received symbols.

j	x_1	x_2	x_o	s_1	s_2	S
0	0	0	0	h_1	h_2	h_1+h_2
1	0	1	1	h_1	$-h_2$	h_1-h_2
2	1	0	1	$-h_1$	h_2	$-h_1+h_2$
3	1	1	0	$-h_1$	$-h_2$	$-h_1-h_2$

$$\begin{cases} L_{k,1}=\ln\left(\dfrac{p_{k,0}+p_{k,2}}{p_{k,1}+p_{k,3}}\right), \\ L_{k,2}=\ln\left(\dfrac{p_{k,0}+p_{k,1}}{p_{k,2}+p_{k,3}}\right), \\ L_{k,o}=\ln\left(\dfrac{p_{k,0}+p_{k,3}}{p_{k,1}+p_{k,2}}\right) \end{cases} \tag{16}$$

According to Eqs. (13) and (16), the input LLR values to decode the longer codeword $x_{1,B}^N=\left(x_{1,o}^Z, x_{1,2}^Z\right)$ can be obtained by

$$\hat{L}_l=\begin{cases} L_{l,o}, & \text{if } 1\leqslant l\leqslant Z, \\ L_{l-Z,2}, & \text{if } Z<l\leqslant N \end{cases} \tag{17}$$

The LLR vector $\hat{L}_1^N=(L_{1,o},\ \ldots,\ L_{Z,o},\ L_{1,2},\ \ldots,\ L_{Z,2})$ will input to a PA-BP decoder that concatenates two length-Z normal BP decoders through an virtual PE, which is shown in Fig. 3. The connection of PE represents the multiplication of codewords and joint matrix $\bar{G}_M$. Finally, the estimated values of $\hat{u}_{1,1}^Z$ and $\hat{u}_{1,2}^Z$ are obtained simultaneously.

3.2 ICA-BP algorithm

Polar code with BP decoding benefits from the application of an outer CRC code, which can enhance the error correcting performance while terminate iterations in advance. CRC code involves the use of polynomial division to create a check value from the information source[36]. In this two-user system, each user has the ability to generate a unique CRC code tailored to their individual message. Thus, the CRC in PA-BP decoder for longer polar code $x_{1,B}^N$ terminates its iterations only when the CRC checks for all estimated user messages satisfy.

During PA-BP decoding, however, some of the users may satisfy CRC condition early. Based on this phenomenon, ICA-BP decoding is proposed, where users having passed the CRC detection earlier can assist decoding other user decoding via IC technique. It can improve the overall error performance for PA-BP decoder in subsequent iterations.

In a two-user system, when the estimated value of a user, either $\hat{u}_{1,1}^Z$ or $\hat{u}_{1,2}^Z$ satisfies the CRC, it is subtracted from the received signal. This subtraction allows for the recalculation of LLR values for the second user and new LLR values will be fed into BP decoder. For example, if user-1 first satisfies the CRC condition, IC and LLR recalculation are performed respectively,

$$\hat{r}_{1,2}^Z=y_1^Z-(1-2\hat{u}_{1,1}^Z G_{N/2}) \tag{18}$$

$$\hat{L}_{1,2}^Z=\frac{2h_2\hat{r}_{1,2}^Z}{\sigma^2} \tag{19}$$

Then, $\hat{L}_{1,2}^Z$ will update the lower half of input LLRs. Similar operation can be done for another circumstance. It is notable that the updated LLRs consist of $L_{1,o}^Z$ and $L_{1,2}^Z$, excluding $L_{1,1}^Z$.

However, given that the nodes with odd indices in the n-th stage of factor graph can be regarded as the XOR result of $x_{1,o}^Z$ and $x_{1,2}^Z$, i.e., $x_{1,1}^Z=x_{1,o}^Z\oplus x_{1,2}^Z$, the recalculated LLR $\hat{L}_{1,1}^Z$ will replace LLRs for these odd nodes. Therefore, convergence of ICA-BP decoder can be accelerated and enhanced by updating the LLR values during iterations. The detailed description of ICA-BP decoder is provided in Algorithm 1 and its framework is shown in Fig. 4. Note that in Algorithm 1, the initial value of variable "flag" is set to 0. When the estimated value of user-2 passes the CRC check, we update $\boldsymbol{L}_{n,j}$ $(0\leqslant j\leqslant Z)$ with the recalculated LLR $\hat{L}_{1,1}^Z$ and set "flag" to 1. This indicates that $\boldsymbol{L}_{n,j}$ have been upgraded by IC. Therefore, in the next left propagation, ICA-BP decoder will not upgrade $\boldsymbol{L}_{n,j}$.

3.3 Code construction

In a two-user uplink NOMA, we encode the polar code of each user into a longer codeword and compute its initial LLRs using Eqs. (16) and (17). Monte Carlo simulations are performed between two users and BS to select the optimal information set. As presented in Algorithm 2, by accumulating the number of errors per bit in the concatenated information block $\hat{u}_1^N=\left(\hat{u}_{1,1}^Z, \hat{u}_{1,2}^Z\right)$, the K of N bit-channels with the lowest error probability are selected as an information set $\mathcal{A}_P$[37]. This set is divided into two subsets $\mathcal{A}_{P,1}$ and

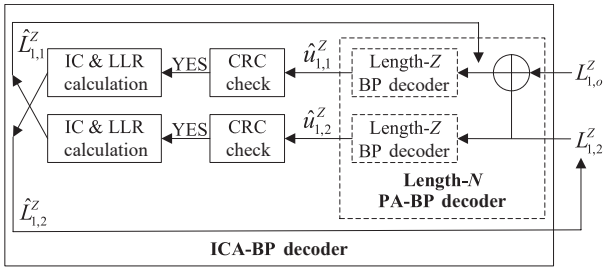

Fig. 4 Framework of ICA-BP decoder.

Algorithm 1 ICA-BP decoder

Input: A, A^c, $L^Z_{1,o}$, $L^Z_{1,2}$, T_{max}, h_1, h_2, H_{crc}
Output: $\hat{u}^Z_{1,1}$, $\hat{u}^Z_{1,2}$
Initialize $\boldsymbol{L}_{n+1,j} \leftarrow (L^Z_{1,o}, L^Z_{1,2})\, j = 1, 2, ..., N$,
$R_1, A^c \leftarrow \infty$, $T \leftarrow 0$, $n \leftarrow \log_2 N + 1$, $flag \leftarrow 0$
while $T < T_{max}$ **do**
  for $i = n : 1$ **do**
    for $j = 1 : N/2$ **do**
      if $flag = 1 \& i = n$ **then**
        Update $\boldsymbol{L}_{i,j+2^{n-1-i}}$ by Eq. (8);
      else
        Update $\boldsymbol{L}_{i,j}$, $\boldsymbol{L}_{i,j+2^{n-1-i}}$ by Eq. (8);
  for $i = 1 : n$ **do**
    for $j = 1 : N/2$ **do**
      Update $R_{i+1,j}$, $R_{i+1,j+2^{n-1-i}}$ by Eq. (9);
  Compute $\hat{u}_j$ by (11), for $j = 1, 2, ..., N$;
  Obtain $\hat{u}^Z_{1,1}$ and $\hat{u}^Z_{1,2}$ from $\hat{u}^N_1$;
  if $u^Z_{1,1} H_{crc} = 0$ & $u^Z_{1,2} H_{crc} = 0$ **then**
    break;
  else if $u^Z_{1,1} H_{crc} = 0$ **then**
    $\hat{L}^Z_{1,2} \leftarrow \frac{2h_2[y^Z_1 - (1-2u^Z_{1,1}G_{N/2})]}{\sigma^2}$;
    $\boldsymbol{L}_{n+1,j+Z} \leftarrow \hat{L}_{j,2}$ for $j = 1, 2, ..., Z$;
  else if $u^Z_{1,2} H_{crc} = 0$ **then**
    flag $\leftarrow 1$;
    $\hat{L}^Z_{1,1} \leftarrow \frac{2h_1[y^Z_1 - (1-2\hat{u}^Z_{1,2}G_{N/2})]}{\sigma^2}$;
    $\boldsymbol{L}_{n,j} \leftarrow \hat{L}_{j,1}$ for $j = 1, 2, ..., Z$;
return the decoded message $\hat{u}^Z_{1,1}$ and $\hat{u}^Z_{1,2}$

Algorithm 2 Monte Carlo construction for two-user

Input: Z, K, h_1, h_2, T_{runs}
Output: $A_{P,1}$, $A_{P,2}$, K_1, K_2
Initialize $N \leftarrow 2Z$, $G_{N/2} \leftarrow F^{\otimes n-1}$, $\mu \leftarrow 0$
for $t = 1 : T_{runs}$ **do**
  $(u^Z_{1,1}, u^Z_{1,2}) \leftarrow$ BitGenerator (N, K);
  $u^N_1 \leftarrow (u^Z_{1,1}, u^Z_{1,2})$;
  $x^Z_{1,1} \leftarrow u^Z_{1,1} G_{N/2}$;
  $x^Z_{1,2} \leftarrow u^Z_{1,2} G_{N/2}$;
  $y^Z_1 \leftarrow h_1 (1 - 2x^Z_{1,1}) + h_2 (1 - 2x^Z_{1,2}) + \eta$;
  Obatin input LLR $\hat{L}^N_1$ using Eqs. (15), (16), (17)
  $\hat{u}^N_1 \leftarrow$ BP Decoder (N, K, L^N_1);
  $\lambda_{err} \leftarrow$ XOR $(u^N_1, \hat{u}^N_1)$;
  $\mu \leftarrow \mu + \lambda_{err}$;
Sort μ and select K of the least erroneous positions to form bit set A_S
for $i = 1 : N$ **do**
  $A_{P,1} \leftarrow A_S\, (i \leqslant Z)$, $A_{P,2} \leftarrow A_S\, (i \geqslant Z + 1)$;
$K_1 \leftarrow |A_{P,1}|$, $K_2 \leftarrow |A_{P,2}|$;
return the information set $A_{P,1}$ and $A_{P,2}$

$\mathcal{A}_{P,2}$ for each user. The user with superior channel condition is allocated a larger share of information bits, leading to adaptive code rate allocation as $(R_1, R_2) = (K_1/Z, K_2/Z)$ for the two users.

To demonstrate the advantage of proposed PA-BP decoding scheme, a longer polar code with a length of $N = 512$ is constructed using Monte Carlo simulation. The symmetric capacity of this code is then compared with that of two shorter polar codes utilizing the conventional SIC scheme, each with a length of $Z = 256$. Figure 5 indicates that PA-BP decoding results in more bit-channels becoming noiseless with capacity tends to one, while the remaining channels degrade into worst channels with zero capacity. It means that the PA-BP decoder benefit from more significant polarization effect.

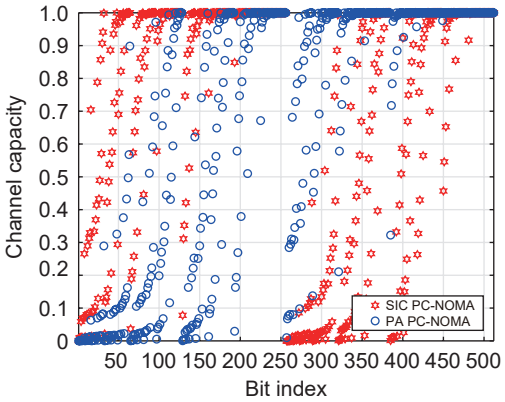

Fig. 5 Comparisons of bit-channels' capacities between SIC-BP scheme and PA-BP decoding scheme with Monte Carlo method.

4 Performance Analysis

4.1 Capacity analysis for two-user NOMA

In a two-user polar-coded uplink NOMA system, each user is encoded into a length-Z polar code, where $N = 2Z$. Upon receiving the superimposed signal y^Z_1, the transmitted codewords are decoded sequentially using SIC decoder. We assume that the channel responses obey

$$|h_1| < |h_2| \tag{20}$$

which means user 1, 2 are weak user and strong user, respectively. Therefore, we first calculate LLR for the 2-nd user and put it into polar decoder. After obtaining the estimated information $\hat{u}^Z_{1,2}$, the codeword of the 2-nd user is re-encoded by a $N/2 \times N/2$ generator matrix $G_{N/2}$

$$\bar{\hat{x}}_{1,2}^{Z} = \hat{u}_{1,2}^{Z} \cdot G_{N/2} \tag{21}$$

Then, $\bar{\hat{x}}_{1,2}^{Z}$ is subtracted from the received signals by SIC, i.e.,

$$\bar{y}_{1,1}^{Z} = y_1^Z - h_2 \cdot \left(1 - 2\bar{\hat{x}}_{1,2}^{Z}\right) \tag{22}$$

Thus, we can ensure that every user achieves the maximum signal-to-interference-plus-noise ratio (SINR).

Assume that the channel state $\boldsymbol{H}$ is known. Thus, the capacity of SIC-BP decoding is represented by

$$I_S\left(y_1^Z; \hat{x}_1^N|\boldsymbol{H}\right) = \sum_{k=1}^{2} I\left(y_1^Z; \hat{x}_{(k-1)Z+1}^{kZ}|\bar{\hat{x}}_1^{(k-1)Z}, \boldsymbol{H}\right) = I\left(y_1^Z; \hat{x}_1^Z|\bar{\hat{x}}_{Z+1}^{2Z}, \boldsymbol{H}\right) + I\left(y_1^Z; \hat{x}_{Z+1}^{2Z}|\boldsymbol{H}\right) \tag{23}$$

However, for PA-BP scheme, since the codewords of all users are jointly encoded by $\bar{G}_M$, the channel capacity can be calculated by

$$I_P\left(y_1^Z; \hat{x}_1^N|\boldsymbol{H}\right) = I\left(y_1^Z; \hat{x}_1^N \cdot \bar{G}_M|\boldsymbol{H}\right) = I\left(y_1^Z; \hat{x}_1^Z \oplus \hat{x}_{Z+1}^{2Z}|\hat{x}_{Z+1}^{2Z}, \boldsymbol{H}\right) + I\left(y_1^Z; \hat{x}_{Z+1}^{2Z}|\boldsymbol{H}\right) \tag{24}$$

According to the cut-set theorem[38, 39], we have

$$I\left(y_1^Z; \hat{x}_1^Z \oplus \hat{x}_{Z+1}^{2Z}|\hat{x}_{Z+1}^{2Z}, \boldsymbol{H}\right) = \min\{I_1, I_2\} \tag{25}$$

where

$$I_1 = I\left(y_1^Z; \hat{x}_1^Z|\bar{\hat{x}}_{Z+1}^{2Z}, \boldsymbol{H}\right) \tag{26}$$

$$I_2 = I\left(y_1^Z; \hat{x}_{Z+1}^{2Z}|\bar{\hat{x}}_1^{Z}, \boldsymbol{H}\right) \tag{27}$$

We can infer that $\min\{I_1, I_2\} = I_1$. Therefore, from Eq. (25), we can deduce that

$$I\left(y_1^Z; \hat{x}_1^Z \oplus \hat{x}_{Z+1}^{2Z}|\hat{x}_{Z+1}^{2Z}, \boldsymbol{H}\right) = I\left(y_1^Z; \hat{x}_1^Z|\bar{\hat{x}}_{Z+1}^{2Z}, \boldsymbol{H}\right) \tag{28}$$

In this case, the channel capacities calculated by Eqs. (23) and (24) for a two-user NOMA are equivalent

$$I_S\left(y_1^Z; \hat{x}_1^N|\boldsymbol{H}\right) = I_P\left(y_1^Z; \hat{x}_1^N|\boldsymbol{H}\right) \tag{29}$$

Thus, both SIC-BP and PA-BP have the same channel capacity in spite of their distinct decoder structures theoretically.

In terms of the code construction, in PA-BP decoding scheme the information set $\mathcal{A}_P$ is initially constructed by treating two users as an integral and then divide $\mathcal{A}_P$ into two parts for users, i.e., $\mathcal{A}_P = (\mathcal{A}_{P,1}, \mathcal{A}_{P,2})$. However, in SIC scheme each user acquires their respective information set $\mathcal{A}_{S,1}$ and $\mathcal{A}_{S,2}$ independently. The capacities of information bits for SIC-BP and PA-BP are given by

$$I_{S,\mathcal{A}_S} = \sum_{k=1}^{2} \sum_{i \in \mathcal{A}_{S,k}} I\left(W_{Z,k}^{(i)}\left(y_1^Z, \hat{u}_{(k-1)Z+1}^{(k-1)Z+i-1}|\bar{\hat{x}}_1^{(s-1)Z}, u_{(k-1)Z+i}\right)\right) \tag{30}$$

$$I_{P,\mathcal{A}_P} = \sum_{i \in \mathcal{A}_P} I\left(W_N^{(i)}\left(y_1^N, \hat{u}_1^{i-1}|u_i\right)\right) \tag{31}$$

Since polarization effect becomes more significant as code length increases and achieve perfect SIC is challenging, PA-BP decoding will attain higher information-bit rate than SIC-BP, i.e., $I_{P,\mathcal{A}_P} > I_{S,\mathcal{A}_S}$.

4.2 EXIT chart analysis

The concept of EXIT chart aims to predict the convergence behavior of iterative decoder by observing the input/output extrinsic information[40]. For iterative decoders, the probability density functions (PDF) of the extrinsic output values E approaches Gaussian-like distributions after running multiple iterations[41].

Take Rayleigh fading channel as an example, with the known transmitted symbol $x \in \{+1, -1\}$, the received a priori LLR value A that to be fed into a BP decoder can be written as

$$A = \lambda_A \cdot x + \eta_A \tag{32}$$

where the Gaussian random variable $\eta_A \sim \mathcal{CN}\left(0, \sigma_A^2\right)$. For the LLR value A, its mean value λ_A satisfies $\lambda_A = \sigma_A^2 h^2/2$ and the variance $\sigma_A^2 = 4/\sigma_n^2$, where h and σ_n^2 denote the Rayleigh channel response and Gaussian noise variance respectively. Moreover, assuming ξ is once observation of x, the conditional PDF of A is

$$p_A(\xi|X = x) = \frac{1}{\sqrt{2\pi}\sigma_A} \exp\left(-\frac{\left(\xi - \frac{\sigma_A^2 h^2}{2} x\right)^2}{2\sigma_A^2}\right) \tag{33}$$

Given the consistency condition and the proof[40, 42], the PDF of L-value A satisfies

$$p_A(\xi|X = x) = p_A(-\xi|X = x) \cdot \mathrm{e}^{xh^2\xi} \tag{34}$$

Thus, by using Eq. (34), we can define the mutual information $I_A = (X; A)$ as

$$I_A = \frac{1}{2} \sum_{x \in \{\pm 1\}} \int_{-\infty}^{+\infty} p_A(\xi|X = x) \cdot \log_2 \frac{2 \cdot p_A(\xi|X = x)}{p_A(\xi|X = -1) + p_A(\xi|X = 1)} \mathrm{d}\xi = 1 - \int_{-\infty}^{+\infty} \frac{\mathrm{e}^{-\left(\left(\xi - \sigma_A^2 h^2/2\right)/2\sigma_A^2\right)}}{\sqrt{2\pi}\sigma_A} \cdot \log_2\left(1 + \mathrm{e}^{-\xi}\right) \mathrm{d}\xi \tag{35}$$

For abbreviation, the functional relation between the

mutual information I_A and variance σ_A can be denoted as

$$I_A(\sigma=\sigma_A):=J(\sigma_A) \tag{36}$$

Since the function $J(\sigma)$ is monotonically increasing and therefore reversible, we have its inverse function that fulfills

$$\sigma_A=J^{-1}(I_A) \tag{37}$$

Taking A as the input LLR values, BP decoder outputs its extrinsic LLR values E at the end of iteration. The associated mutual information $I_E=(X;E)$ can be calculated by

$$I_E=\frac{1}{2}\sum_{x\in\{\pm1\}}\int_{-\infty}^{+\infty}p_E(\xi|X=x)\cdot \log_2\frac{2\cdot p_E(\xi|X=x)}{p_E(\xi|X=-1)+p_E(\xi|X=1)}\mathrm{d}\xi \tag{38}$$

In general, the distributions p_E in Eq. (38) are measured using histogram method. Furthermore, we employ an approximation form of Eq. (38) which is convenient for calculation:

$$I_E=1-E\left[\log_2\left(1+\mathrm{e}^{-E_k}\right)\right]\approx 1-\frac{1}{N}\sum_{k=1}^{N}\log_2\left(1+\mathrm{e}^{-x_kE_k}\right) \tag{39}$$

where E_k is the extrinsic LLR values of k-th symbol x_k. I_A and I_E are bounded between 0 and 1. For a certain mutual information value I_A, its associated I_E can be obtained from BP decoder, which means they constitute a one-to-one mapping. This mapping indicates the EXIT characteristics of BP decoder and is derived as

$$I_E=T(I_A) \tag{40}$$

To plot the EXIT chart for iterative decoders, we follow the procedure described in Ref. [43] for both SIC-BP and PA-BP decoders. In brief, we regard the a priori mutual information I_A as a variable increased from 0 to 1 with a small step. Then a certain value of σ_A is determined by Eq. (37). Substitute σ_A to Eq. (32), an associated LLR value A is obtained. BP decoders initialize left message $\boldsymbol{L}_{n+1,j}$ with the LLR value A_j and output extrinsic LLR value $E_j=\boldsymbol{R}_{n+1,j}-\boldsymbol{L}_{n+1,j}$ after many times of iterations. The final step is to compute I_E using the approximated Formula (39).

The EXIT charts for SIC-BP and PA-BP are shown in Fig. 6. It can be observed that as I_A increases, the curves of I_E are also monotonically increasing. I_E finally reaches the theoretical upper bound of $I_E=1.0$, which means faultless decoding. When I_A is constant, the greater I_E means a superior error correcting ability of the decoder. The blue EXIT curve that represents our proposed PA-BP decoding scheme surpasses the red curve of SIC across all ranges of I_A which shows superior error correcting ability. Furthermore, PA-BP is the first to reach the upper bound of $I_E=1.0$ which signifies a faster convergence speed than SIC-BP.

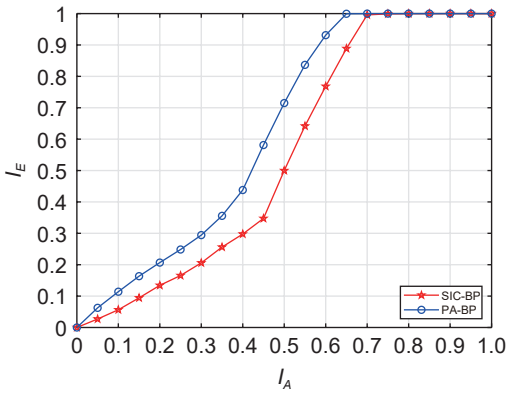

Fig. 6 Extrinsic information transfer characteristics of SIC-BP and PA-BP decoders for code rate $R=1/2$.

5 Simulation Result

In this section, we perform simulations of the proposed PA-BP, ICA-BP, and SIC-BP decoder over Gaussian and Rayleigh fading channels, $h_1<h_2$. For a two-user NOMA system, we set the fixed channel response $(h_1, h_2)=(0.8, 1.0)$ to denote weak and strong users respectively in GMAC. For Rayleigh fading channel, we set channel distances as $(d_1, d_2)=(10, 5)$ and assign path loss exponent $\gamma=0.5$. The codeword length $Z=256$ for transmit users and then the constructed long polar code at the receiver has the length of $N=512$. Using Monte Carlo code construction, code rates of two users are allocated as $(R_1, R_2)=(0.31, 0.69)$ which maintains an overall system rate $R=0.5$ for NOMA. Additionally, 16-bits CRC codes are generated for each user using the generator polynomial $g(x)=x^{16}+x^{12}+x^5+1$. The maximum number of BP iterations is set to 50. Moreover, we not only perform BP decoding but also simulate SC decoding as a benchmark.

5.1 Performance of construction optimization

Figure 7 compares the BER performance of PA-BP decoding for different construction methods. The PA-BP with proposed Monte-Carlo construction has a

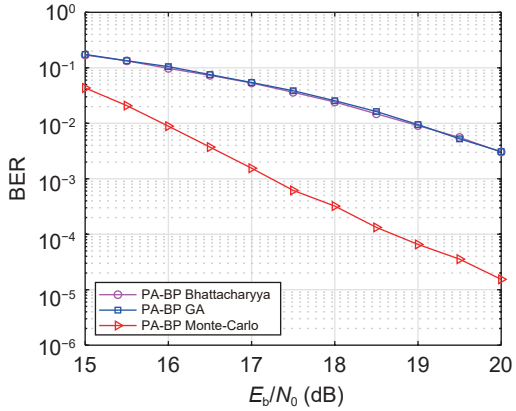

Fig. 7 BER performance of PA-BP decoding for different construction methods over Rayleigh fading channel with $N = 512$.

significant performance gain of 3 dB over Bhattacharyya parameter[11] and GA methods at BER of 10^{-2} in NOMA with fading channels, which validates the advantages of the proposed code optimization method.

5.2 Performance of two-user NOMA

Figures 8 and 9 show the BER performance of PA decoding and conventional SIC schemes over different channels. As shown, the PA scheme has a performance gain of 1.2 dB over SIC schemes for SC decoder and 0.8 dB for BP decoder at BER of 10^{-4} in GMAC. From Fig. 9, these gains are 0.6 dB and 0.7 dB respectively in Rayleigh fading channel. Moreover, at a BER of 10^{-4}, ICA-BP further achieves the performance gain of 0.4 dB over PA-BP in GMAC. In Rayleigh fading channel, the gain increases slightly to 0.5 dB.

Figures 10 and 11 compare the average number of iterations to converge by iterative decoders. In both

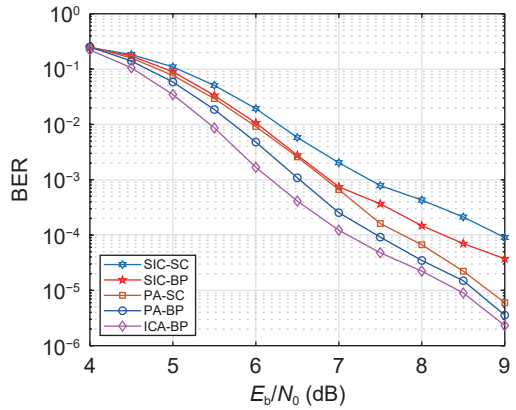

Fig. 8 BER performance of PA and SIC decoders over GMAC with $N = 512$.

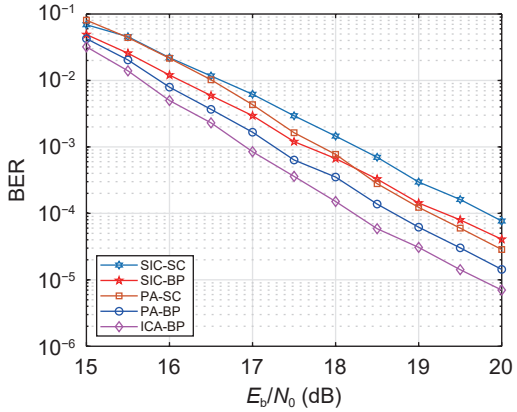

Fig. 9 BER performance of PA and SIC decoders over Rayleigh fading channel with $N = 512$.

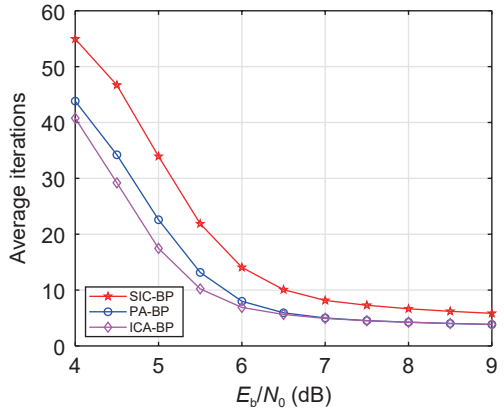

Fig. 10 Average iterations to converge by SIC-BP, PA-BP, and ICA-BP over GMAC.

GMAC and Rayleigh fading channels, PA-BP decoder converges faster than SIC-BP in all simulated E_b/N_0 regions. Specifically, Fig. 10 shows that the PA-BP decoder reduces the iteration number of SIC-BP by one in GMAC. This number reduction is about two in Rayleigh fading channel, as shown in Fig. 11. Furthermore, in low E_b/N_0 region (< 6 dB), ICA-BP decoder shows less iterations than the other schemes in both channels.

Figure 12 further shows the average times of IC performed in ICA-BP decoder. For both GMAC and Rayleigh fading channels, the average IC times are fewer than once in all simulated E_b/N_0 regions and the trends descent as E_b/N_0 increases. Therefore, ICA-BP decoder only introduces minimal latency compared to the PA-BP decoder.

5.3 Complexity performance

We compare the computational complexities of PA and

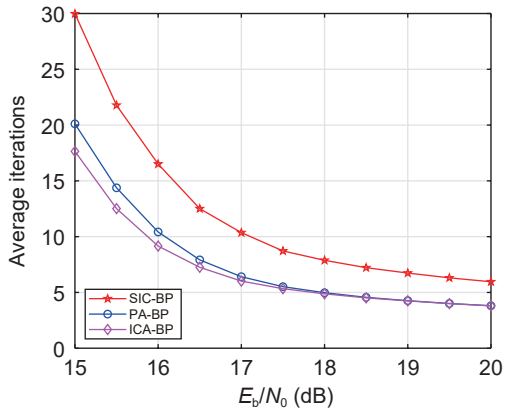

Fig. 11 Average iterations to converge by SIC-BP, PA-BP, and ICA-BP over Rayleigh fading channel.

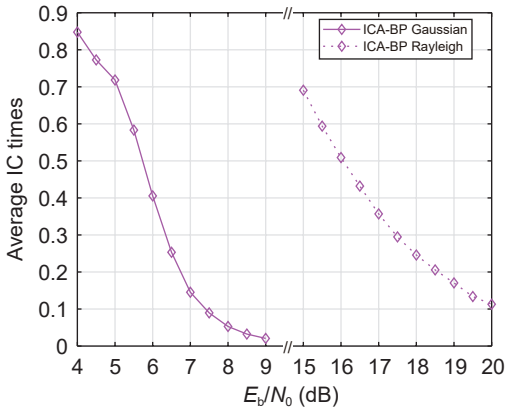

Fig. 12 Average times of IC performed by ICA-BP decoder over GMAC and Rayleigh fading channel. The abscissa at E_b/N_0 = 10-14 dB has been cut off.

SIC schemes, as summarized in Table 2. In this table, T represents the average number of iterations that decoders have consumed and J denotes the average times of IC performed by ICA-BP decoder. T_1 and T_2 are the average number of iterations of two BP decoders for SIC-BP. In PA-SC, we employ the SC decoding for a longer polar with length-N. Thus, the decoding complexity of PA-SC is $\mathcal{O}(N\log_2 N)$. In contrast, SIC-SC utilizes the SIC decoding method for the received signal, which consists of one codeword reconstruction and two SC decoding of the length-$N/2$, leading to the decoding complexity of $\mathcal{O}\left(3\frac{N}{2}\log_2\frac{N}{2}\right)$. It means that as compared to SIC-SC, PA-SC incurs no additional cost. With regard to BP decoding, the complexity mainly depends on the number of iterations. Compared with PA-BP, the ICA-BP decoder requires an additional complexity of $\mathcal{O}\left(J\frac{N}{2}\log_2\frac{N}{2}\right)$ due to the J times encoding followed by J times IC.

Table 2 Analyses of decoding complexity.

	PA decoder	SIC decoder
SC	$\mathcal{O}(N\log_2 N)$	$\mathcal{O}\left(3\frac{N}{2}\log_2\frac{N}{2}\right)$
BP	$\mathcal{O}(TN\log_2 N)$	$\mathcal{O}\left((T_1+T_2+1)\frac{N}{2}\log_2\frac{N}{2}\right)$
ICA-BP	$\mathcal{O}\left(TN\log_2 N+J\frac{N}{2}\log_2\frac{N}{2}\right)$	-

To make the comparisons in Table 2 more intuitive, we give the number of arithmetic operations with T and J measured in the simulations. As shown in Figs. 13 and 14, PA-SC has less operations than SIC-SC for simulated E_b/N_0 regions in both channels. The computational complexity difference between PA-SC and SIC-SC seems negligible for $N = 512$. However, as the code length increases, this difference becomes significant. Meanwhile, PA-BP requires much more operations in low E_b/N_0 region compared with SIC-BP, but the gap is narrowed as E_b/N_0 increases. Moreover, although the proposed PA-BP has a slightly higher complexity, it achieves much better decoding performance than the latter one. Due to the faster convergence, ICA-BP can reduce the operations of PA-BP in both channels.

5.4 Performance of list decoding

To explore the potential advantages of list decoding for proposed ICA-BP, we form ICA-BPL decoding, which implements ICA-BP decoding across various permuted factor graphs[44]. The list decoding for PA scheme are also introduced as benchmarks[45, 46], i.e., PA-BPL, PA-SCL, and PA-CA-SCL, which perform BPL, SCL, and CA-SCL based on PA decoder. To ensure a fair comparison, all the list algorithms are assigned the

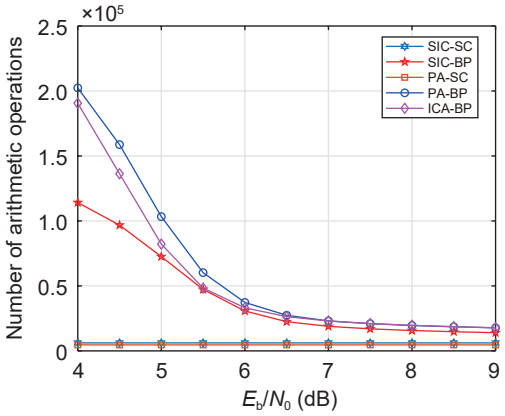

Fig. 13 Number of arithmetic operations for different algorithms over GMAC with N = 512.

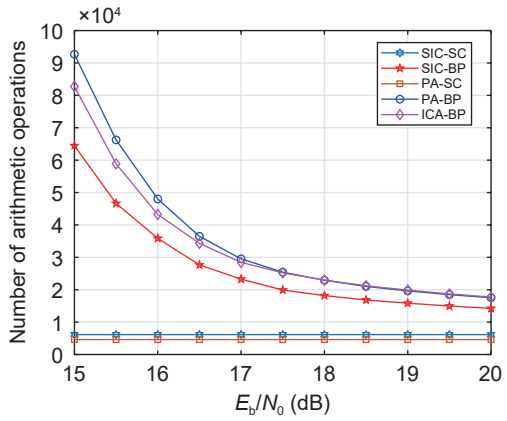

Fig. 14 Number of arithmetic operations for different algorithms over Rayleigh fading channel with $N = 512$.

same list size of $L = 8$ and 16-bits CRC code using the generator polynomial $g(x) = x^{16} + x^{12} + x^5 + 1$. We design the permuted factor graphs with the upper bound method proposed in Ref. [47].

Figures 15 and 16 demonstrate that ICA-BPL outperforms PA-BPL and PA-SCL, but there still exist a performance gap away from PA-CA-SCL. In GMAC, at BER of 10^{-5}, ICA-BPL outperforms PA-BPL and PA-SCL by 0.65 dB and 0.5 dB, respectively, while suffers a performance loss of 0.3 dB as compared to PA-CA-SCL. Moreover, in Rayleigh fading channel, at BER of 10^{-5}, ICA-BPL achieves gains of 0.65 dB and 0.35 dB over PA-BPL and PA-SCL, respectively. Also, PA-CA-SCL performs best among all the schemes.

6 Conclusion

In this paper, we propose a PA-BP decoding for uplink NOMA to improve the non-optimal performance of SIC decoder at finite block length. By exploiting the properties of polar coding, the receiver virtually constructs a long codeword and the user codes are seen as its nested codes. We then utilize Monte Carlo construction to optimize the bit-information set and allocate user code rates with the different channels. We further propose an ICA-BP decoder to enhance the performance of PA-BP. The EXIT chart and simulation results show that the PA decoder achieves superior performance to the SIC counterparts for both SC and BP algorithms. Moreover, the proposed ICA-BP has less computational complexity and obtains additional performance gain over the PA-BP. For list decoding, the ICA-BPL also performs better than PA-BPL and PA-SCL, but is yet inferior to PA-CA-SCL.

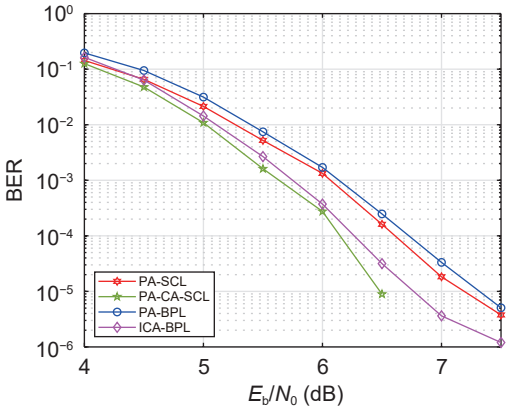

Fig. 15 BER performance comparisons of list decoding over GMAC with $N = 512$.

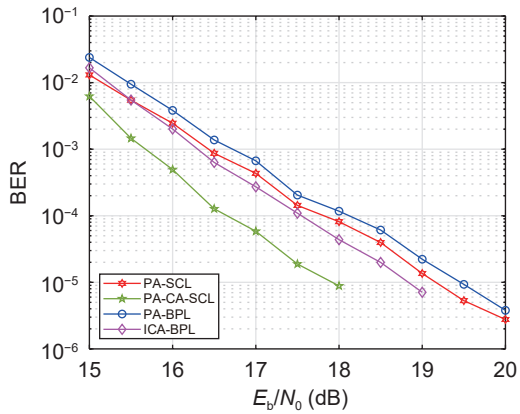

Fig. 16 BER performance comparisons of list decoding over Rayleigh fading channel with $N = 512$.

Acknowledgment

The work was supported by the National Natural Science Foundation of China (No. 62171135), Fujian Distinguished Talent Project (No. 2022J06010), Fujian Province Key Technique Project (No. 2023XQ004), and Fuzhou Science and Technology Planning Project (No. 2023-P-001).

References

[1] K. Higuchi and A. Benjebbour, Non-orthogonal multiple access (NOMA) with successive interference cancellation for future radio access, *IEICE Trans. Commun.*, vol. E98.B, no. 3, pp. 403–414, 2015.

[2] D. Zhai, R. Zhang, L. Cai, B. Li, and Y. Jiang, Energy-efficient user scheduling and power allocation for NOMA-based wireless networks with massive IoT devices, *IEEE Internet Things J.*, vol. 5, no. 3, pp. 1857–1868, 2018.

[3] S. Timotheou and I. Krikidis, Fairness for non-orthogonal multiple access in 5G systems, *IEEE Signal Process. Lett.*, vol. 22, no. 10, pp. 1647–1651, 2015.

[4] O. Dizdar, C. Goken, and A. Yilmaz, An uplink non-

orthogonal multiple access method based on frozen bit patterns of polar codes, *IEEE Commun. Lett.*, vol. 23, no. 6, pp. 975–978, 2019.

[5] L. Yuan, J. Pan, N. Yang, Z. Ding, and J. Yuan, Successive interference cancellation for LDPC coded non-orthogonal multiple access systems, *IEEE Trans. Veh. Technol.*, vol. 67, no. 6, pp. 5460–5464, 2018.

[6] H. Cui, K. Niu, M. Ren, and J. Huo, Polar coded power domain non-orthogonal multiple access system: Construction and optimization, *IEEE Commun. Lett.*, vol. 28, no. 3, pp. 607–611, 2024.

[7] L. Dai, B. Wang, Y. Yuan, S. Han, I. Chih-lin, and Z. Wang, Non-orthogonal multiple access for 5G: solutions, challenges, opportunities, and future research trends, *IEEE Commun. Mag.*, vol. 53, no. 9, pp. 74–81, 2015.

[8] T. Park, G. Lee, W. Saad, and M. Bennis, Sum rate and reliability analysis for power-domain non-orthogonal multiple access (PD-NOMA), *IEEE Internet Things J.*, vol. 8, no. 12, pp. 10160–10169, 2021.

[9] M. T. P. Le, L. Sanguinetti, E. Björnson, and M.-G. D. Benedetto, Code-domain NOMA in massive MIMO: When is it needed?, *IEEE Trans. Veh. Technol.*, vol. 70, no. 5, pp. 4709–4723, 2021.

[10] Y. Zhang, H. M. Wang, T.-X. Zheng, and Q. Yang, Energy-efficient transmission design in non-orthogonal multiple access, *IEEE Trans. Veh. Technol.*, vol. 66, no. 3, pp. 2852–2857, 2017.

[11] E. Arikan, Channel polarization: A method for constructing capacity-achieving codes for symmetric binary-input memoryless channels, *IEEE Trans. Inf. Theory*, vol. 55, no. 7, pp. 3051–3073, 2009.

[12] E. Arikan, Systematic polar coding, *IEEE Commun. Lett.*, vol. 15, no. 8, pp. 860–862, 2011.

[13] K. D. Rao, Performance analysis of enhanced turbo and polar codes with list decoding for uRLLC in 5G systems, in *Proc. 2019 IEEE Int. Conf. for Converg. Technol.* (*I2CT*), Pune, India, 2019, pp. 1–6.

[14] J. Mandelbaum, S. Miao, N. A. Schwendemann, H. Jäkel, and L. Schmalen, Improved generalized automorphism belief propagation decoding, arXiv preprint arXiv: 2406.02012, 2024.

[15] C. F. Teng and A. Y. Wu, A 7.8-13.6 pj/b ultra-low latency and reconfigurable neural network-assisted polar decoder with multi-code length support, *IEEE Trans. Circuits Syst. I, Reg. Papers*, vol. 68, no. 5, pp. 1956–1965, 2021.

[16] R. Zhang, F. Liu, Z. Zeng, Q. Shang, and S. Zhao, Neural network based successive cancellation decoding algorithm for polar codes in uRLLC, in *Proc. 16th Int. Symp. Wireless Commun. Syst.* (*ISWCS*), Oulu, Finland, 2019, pp. 182–187.

[17] E. Arikan, Polar codes: A pipelined implementation, in *Proc. 4th Int. Symp. Broadcast. Commun* (*ISBC*), Melaka, Malaysia, 2010, pp. 11–14.

[18] J. Dai, K. Niu, Z. Si, C. Dong, and J. Lin, Polar-coded non-orthogonal multiple access, *IEEE Trans. Signal Process.*, vol. 66, no. 5, pp. 1374–1389, 2018.

[19] S. He, Q. Zhang, and J. Qin, Joint multi-user decoding for polar-coded uplink non-orthogonal multiple access systems, *IEEE Wireless Commun. Lett.*, vol. 11, no. 1, pp. 72–76, 2022.

[20] Z. Xie, P. Chen, and Y. Li, Joint design of polar coding and physical network coding for two- user downlink non-orthogonal multiple access, *Entropy*, vol. 25, no. 2, pp. 233, 2023.

[21] Z. Xie, P. Chen, Z. Mei, S. Long, K. Cai, and Y. Fang, Polar-coded physical layer network coding over two-way relay channels, *IEEE Commun. Lett.*, vol. 23, no. 8, pp. 1301–1305, 2019.

[22] C. Huang, P. Chen, Z. Xie, and Y. Fang, Improving LDPC-coded PNC decoders via informed dynamic scheduling, *IEEE Commun. Lett.*, vol. 27, no. 8, pp. 1949–1953, 2023.

[23] Z. Xie, P. Chen, R. Chen, and Y. Fang, Polar coded modulation operated with physical network coding, *IEEE Signal Process. Lett.*, vol. 28, pp. 997–1001, 2021.

[24] X. Xie, P. Chen, Y. Fang, and Z. Xie, Low complexity majority-logic decoding for LDPC-coded PNC systems, *IEEE Commun. Lett.*, vol. 26, no. 5, pp. 959–963, 2022.

[25] J. Cui, Z. Ding, and P. Fan, A novel power allocation scheme under outage constraints in NOMA systems, *IEEE Signal Process. Lett.*, vol. 23, no. 9, pp. 1226–1230, 2016.

[26] V. Lau, Y. Liu, and T. A. Chen, Capacity of memoryless channels and block-fading channels with designable cardinality-constrained channel state feedback, *IEEE Trans. Inf. Theory*, vol. 50, no. 9, pp. 2038–2049, 2004.

[27] C. Luo, J. Ji, Q. Wang, X. Chen, and P. Li, Channel state information prediction for 5G wireless communications: A deep learning approach, *IEEE Trans. Netw. Sci. Eng.*, vol. 7, no. 1, pp. 227–236, 2020.

[28] P. Trifonov, Efficient design and decoding of polar codes, *IEEE Trans. Commun.*, vol. 60, no. 11, pp. 3221–3227, 2012.

[29] Y. Chen, X. Qiao, K. Deng, S. Song, and Z. Wang, 3.8-Gbps polar belief propagation decoder on GPU, *IEEE Commun. Lett.*, vol. 27, no. 5, pp. 1247–1251, 2023.

[30] B. Feng, R. Liu, and K. Tian, A novel post-processing method for belief propagation list decoding of polar codes, *IEEE Commun. Lett.*, vol. 25, no. 8, pp. 2468–2471, 2021.

[31] M. Zhang, Z. Li, and L. Xing, An enhanced belief propagation decoder for polar codes, *IEEE Commun. Lett.*, vol. 25, no. 10, pp. 3161–3165, 2021.

[32] H. Liu, E. Gunawan, H. Yaoyue, and Y. L. Guan, BP-based sparse graph list decoding of polar codes, *IEEE Commun. Lett.*, vol. 27, no. 5, pp. 1257–1261, 2023.

[33] B. Yuan and K. K. Parhi, Architecture optimizations for BP polar decoders, in *Proc. 2013 IEEE Int. Conf. Acoust., Speech Signal Process* (*ICASSP*), Vancouver, Canada, 2013 pp. 2654–2658.

[34] B. Yuan and K. K. Parhi, Early stopping criteria for energy-efficient low-latency belief-propagation polar code decoders, *IEEE Trans. Signal Process.*, vol. 62, no. 24, pp. 6496–6506, 2014.

[35] C. Simsek and K. Turk, Simplified early stopping criterion for belief-propagation polar code decoders, *IEEE Commun. Lett.*, vol. 20, no. 8, pp. 1515–1518, 2016.

[36] M. Geiselhart, A. Elkelesh, M. Ebada, S. Cammerer, and S. ten Brink, CRC-aided belief propagation list decoding of polar codes, in *Proc. 2020 IEEE Int. Symp. Inf. Theory* (*ISIT*), Los Angeles, CA, USA, 2020, pp. 395–400.

[37] H. Vangala, E. Viterbo, and Y. Hong, "A comparative study of polar code constructions for the AWGN channel," *arXiv preprint arXiv: 1501.02473*, 2015.
[38] S. Zhang and S. C. Liew, Channel coding and decoding in a relay system operated with physical-layer network coding, *IEEE J. Sel. Areas Commun.*, vol. 27, no. 5, pp. 788–796, 2009.
[39] S. Zhang, S. C. Liew, H. Wang, and X. Lin, "Capacity of two-way relay channel," in *Access Networks*, pp. 219–231, 2010.
[40] S. ten Brink, Convergence behavior of iteratively decoded parallel concatenated codes, *IEEE Trans. Commun.*, vol. 49, no. 10, pp. 1727–1737, 2001.
[41] P. Chen, L. Shi, Y. Fang, F. C. M. Lau, and J. Cheng, Rate-diverse multiple access over Gaussian channels, *IEEE Trans. Wireless Commun.*, vol. 22, no. 8, pp. 5399–5413, 2023.
[42] A. Ashikhmin, G. Kramer, and S. ten Brink, Extrinsic information transfer functions: model and erasure channel properties, *IEEE Trans. Inf. Theory*, vol. 50, no. 11, pp. 2657–2673, 2004.
[43] Z. Q. Chen, L. Li, Z. Ma, and P. Z. Fan, "List selection and decision fusion scheme for belief propagation list decoding of polar codes," in *Proc. 2019 IEEE Inter. Symp. on Personal, Indoor and Mobile Radio Commun.* (*PIMRC*), Istanbul, Turkey, 2019, pp. 1–7.
[44] A. Elkelesh, M. Ebada, S. Cammerer, and S. ten Brink, Belief propagation list decoding of polar codes, *IEEE Commun. Lett.*, vol. 22, no. 8, pp. 1536–1539, 2018.
[45] I. Tal and A. Vardy, List decoding of polar codes, *IEEE Trans. Inf. Theory*, vol. 61, no. 5, pp. 2213–2226, 2015.
[46] K. Niu and K. Chen, CRC-aided decoding of polar codes, *IEEE Commun. Lett.*, vol. 16, no. 10, pp. 1668–1671, 2012.
[47] B. Li, B. Bai, M. Zhu, and S. Zhou, "Improved belief propagation list decoding for polar codes," in *Proc. 2020 IEEE Int. Symp. Inf. Theory* (*ISIT*), Los Angeles, CA, USA, 2020, pp. 1–6.

Yuehui Xu received the BSc degree in electronic information engineering from Fuzhou University, Fujian, China, in 2022. He is currently working towards the MSc degree with College of Physics and Information Engineering. His research interests include polar codes and non-orthogonal multiple access.

Xinyang Piao received the bachelor's degree in telecommunication engineering and management from Beijing University of Posts and Telecommunications in 2012, and the master's degree in electrical engineering from Columbia University, New York, NY, USA, 2014. Her current research areas include wireless communication coding, 5G, 6G, artificial intelligence, and optical communication.

Zhaopeng Xie received the PhD degree in communication and information system from Fuzhou University, Fujian, China, in 2023. He is currently a lecturer with School of Advanced Manufacturing, Fuzhou University, China. His primary research interests include joint source and channel coding, signal processing for wireless communication, channel coding, physical network coding.

Yuanping Wang received the BSc degree in communication engineering from Fuzhou University, Fujian, China, in 2021, where he is currently pursuing the MSc degree with College of Physics and Information Engineering. His research interests include polar codes, spatial modulation, and multiple-input multiple-output wireless communications.

Pingping Chen is currently a professor in Fuzhou University, China. He received the PhD degree in electronic engineering, Xiamen University, China, in 2013. From May 2012 to September 2012, he was a research assistant in electronic and information engineering with The Hong Kong Polytechnic University, China. From January 2013 to January 2015, he was a postdoctoral researcher at the Institute of Network Coding, Chinese University of Hong Kong, China. From July 2016 to July 2017, he was a postdoctoral researcher at Singapore University of Technology and Design. His primary research interests include channel coding, data storage, joint source and channel coding, and network coding.